Rotationally-Resolved Two-Dimensional Infrared Spectroscopy of CO_2(g): Rotational Wavepackets and Angular Momentum Transfer

Kai C. Gronborg, Sydney M. Giles, and Sean Garrett-Roe*

Department of Chemistry, University of Pittsburgh, 219 Parkman Avenue, Pittsburgh, PA 15260, United States

E-mail: sgr@pitt.edu

Phone: +1 412 624 1283. Fax: +1 412 624 8611

Abstract

Angular momentum transfer and wavepacket dynamics of CO_2(g) were measured on the picosecond timescale using polarization-resolved two-dimensional infrared (2D-IR) spectroscopy. The dynamics of rotational levels up to $J_{max} \approx 50$ are observed simultaneously at room temperature. Rotational wavepackets launched by the pump pulses cause oscillations in intensity of individual peaks and beating patterns in the 2D-IR spectra. The structure of the rotationally-resolved 2D-IR spectrum is explained using nonlinear response function theory. Spectral diffusion of the rotationally-resolved 2D-IR peaks reveals information about angular momentum transfer. We demonstrate the ability to directly measure inelastic angular momentum dynamics simultaneously across the ~50 thermally excited rotational levels over several hundred picoseconds.

Graphical TOC Entry

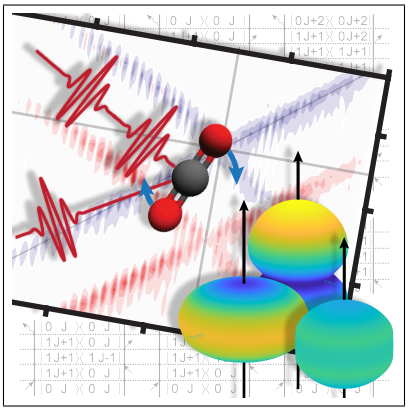

Keywords

ultrafast vibrational spectroscopy, 2D-IR, carbon dioxide, angular momentum transfer, wavepacket dynamics

An early motivation of ultrafast spectroscopy was to complement high-resolution spectroscopies. Where high-resolution spectroscopies could, in principle, determine the eigenstates of a system, often in the gas phase or a cryogenic matrix, with high precision, ultrafast spectroscopy could measure the time-evolution in the condensed phase. The prospect of resolving ultrafast dynamics is not, however, the only possible benefit of ultrafast multi-dimensional spectroscopies. Two-dimensional infrared (2D-IR) spectroscopy is capable of collecting state-specific information about many states simultaneously. 2D-IR spectroscopy coherently excites transitions within the laser band-width and spreads the response over both the pump and probe axes. Here, we show the essential information content in rotationally-resolved rotation-vibration spectroscopy of CO_2(g). The rotationally-resolved spectra show complex structure due to angular momentum selection rules,[1] oscillations in the rotational anisotropy due to interstate coherences, and spectral diffusion due to angular momentum transfer. Here, we use the term "angular momentum transfer" to describe the exchange of angular momentum resulting from inelastic collisions, similar to the use of terms such as J-diffusion,[2] J scrambling,[1] rotational transfer,[3,4] and rotational energy transfer.[5]

2D-IR spectroscopy is a third-order nonlinear vibrational spectroscopy in which two strong pulses (pumps) excite the sample and a third electric field interaction (probe) generates a signal field which is, usually, detected by interfering it with another external field[6] (Figure 1e). The waiting time between the pump and probe pulses, t_2, is varied to observe how the system evolves on the femtosecond to picosecond timescale. The pump pulses produce an initial frequency axis, ω_1, while the response of the system after the probe pulse generates a final frequency axis, ω_3.

Rotational selection rules in the gas phase cause dramatic structure in the 2D-IR lineshape (Figure 1d). In the condensed phase, for example, CO_2 has a simple IR lineshape. The linear absorption spectrum of the antisymmetric stretch, ν_3, shows one band, and the 2D-IR spectrum shows one band from stimulated emission and ground-state bleach (blue) and one band from excited-state absorption (red). In the linear spectrum of the gas phase, however,

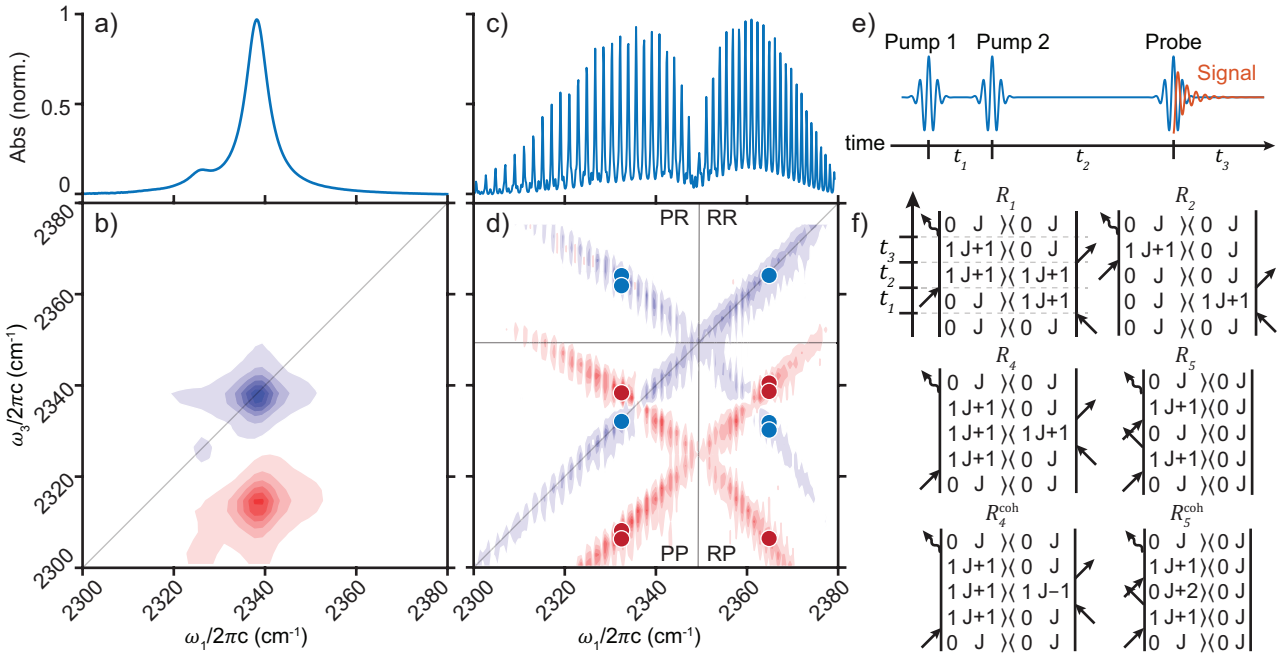

Figure 1: a) In the condensed-phase, e.g. dichloromethane, CO_2 absorbs at 2338 cm^{-1} (the anti-symmetric stretch) and 2326 cm^{-1} (a hot band),[7] which (b) appear in the 2D-IR spectrum of CO_2 as pairs of diagonal peaks. c) The gas-phase FTIR spectrum of CO_2 contains two branches (P and R) centered at ∼2350 cm^{-1} with many rovibrational peaks caused by the rovibrational selections rules. d) The same selection rules lead to the formation of an X-shaped pattern of peaks centered at ∼2350 cm^{-1} that can be separated into four quadrants in the 2D-IR spectrum. e) 2D-IR spectra are produced using two pump pulses, separated by t_1, and a probe pulse separated from pump 2 by t_2. f) The peaks in the RR-quadrant originate in 6 double-sided Feynman diagrams, two of which, R_4^{coh} and R_5^{coh} contain an interstate coherence during t_2. The azimuthal quantum number, m, is suppressed from the diagrams for brevity.

the rotational selection rules for CO_2 lead to sets of transitions in which angular momentum either decreases, $\Delta J = -1$ (P-branch) or increases, $\Delta J = +1$ (R-branch). Because $\Delta J = 0$ is a forbidden transition for CO_2, the Q-branch is absent. As Mandal et al.[1] demonstrated for N_2O, the angular momentum selection rules lead to a dramatic double X-shaped structure in the 2D-IR spectrum of a free rotor (Figure 1d). Molecules starting from a particular angular momentum state can undergo either $\Delta J = \pm 1$ transitions from interactions with the pump and probe pulses. As a result, the spectrum can be divided into four quadrants (Figure 1d) based on the character of the pumped and probed transitions. Additional transitions further up the vibrational ladder lead to similar X-shaped bands, anharmonically shifted to lower values of ω_3. The spacing of the rotational peaks increases in the P-branch and decreases in the R-branch as the initial angular momentum increases, moving away from the (missing) Q-branch, mostly because of rotational-vibrational coupling. Because of this, the peaks appearing in the RP- and PR-quadrants curve toward lower frequency below the anti-diagonal line with increasing J.

In total, molecules can traverse 36 possible pathways up and down the ladder of rotational-vibrational energy levels and can generate 12 possible peaks in a spectrum (Figure 1d, red and blue dots).[1] Given the complexity of the spectrum, we focus on the RR-quadrant of the spectrum, which allows us to restrict the discussion to only 6 of the 36 possible pathways (Figure 1f). These pathways contain both rephasing diagrams (R_1 and R_2) and non-rephasing diagrams (R_4, R_5, R_4^{coh} and R_5^{coh}) following the relevant vibrational and rotational selection rules. An equivalent, generalized approach to theoretically treating the polarization dependence of rotationally-resolved 2D-IR spectra has been recently proposed.[8,9]

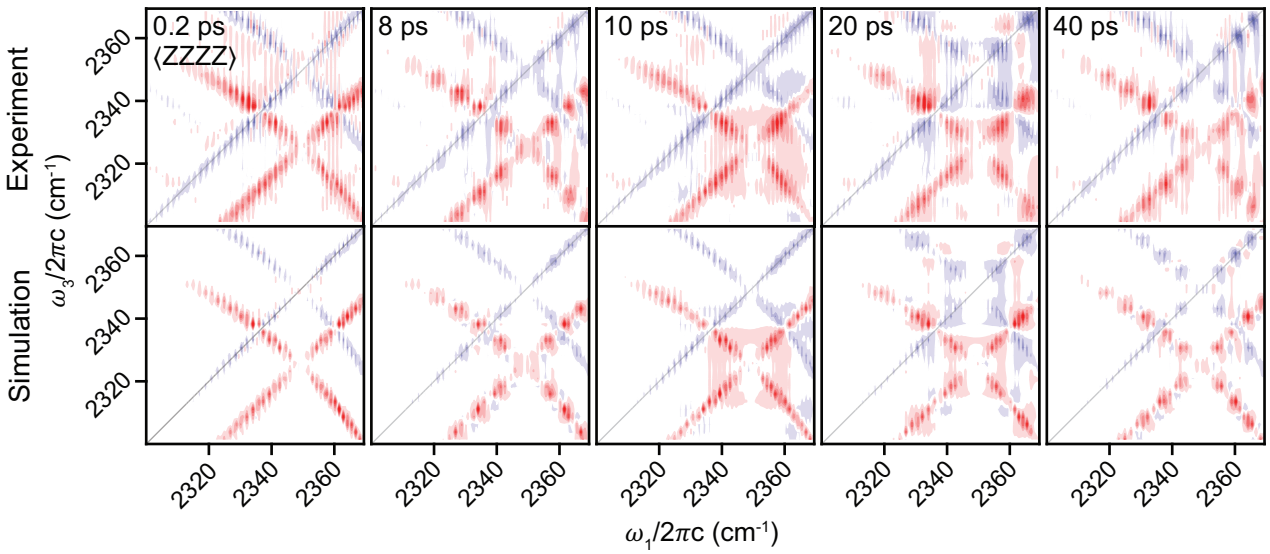

Figure 2: Orientational dynamics cause a beating pattern in the rotationally-resolved spectrum of CO_2(g). Rotational coherences during t_2 cause oscillations in peak intensity in the experimental and simulated 2D-IR spectra.

Because the 2D-IR spectrum of CO_2 is rotationally-resolved, new dynamics become observable (Figure 2, top). At early times, 0.2 ps, the double X-shape is clearly visible. As the waiting time, t_2, increases, however, the spectra develop a strong beating pattern which appears and, then, disappears (Figure 2). The beats become particularly pronounced around 8 ps, 20 ps and 40 ps.

A close examination of 2D-IR spectra with different polarization conditions clarifies that the beating pattern is due to molecular reorientation. At a time-delay of 20 ps, the spectrum collected with all pulses polarized in one direction, S_{ZZZZ}, has a minimum in absolute intensity at 2360 cm^{-1}, whereas the spectrum collected with perpendicular pulses, S_{XXZZ}, has a maximum in absolute intensity (Figure 3a). Molecules initially aligned along the Z-axis have rotated to the X-axis. The rotational anisotropy,

$$\alpha = \frac{S_{ZZZZ} - S_{XXZZ}}{S_{ZZZZ} + 2S_{XXZZ}}, \tag{1}$$

quantifies the degree of rotational alignment. The initially isotropic sample has an anisotropy

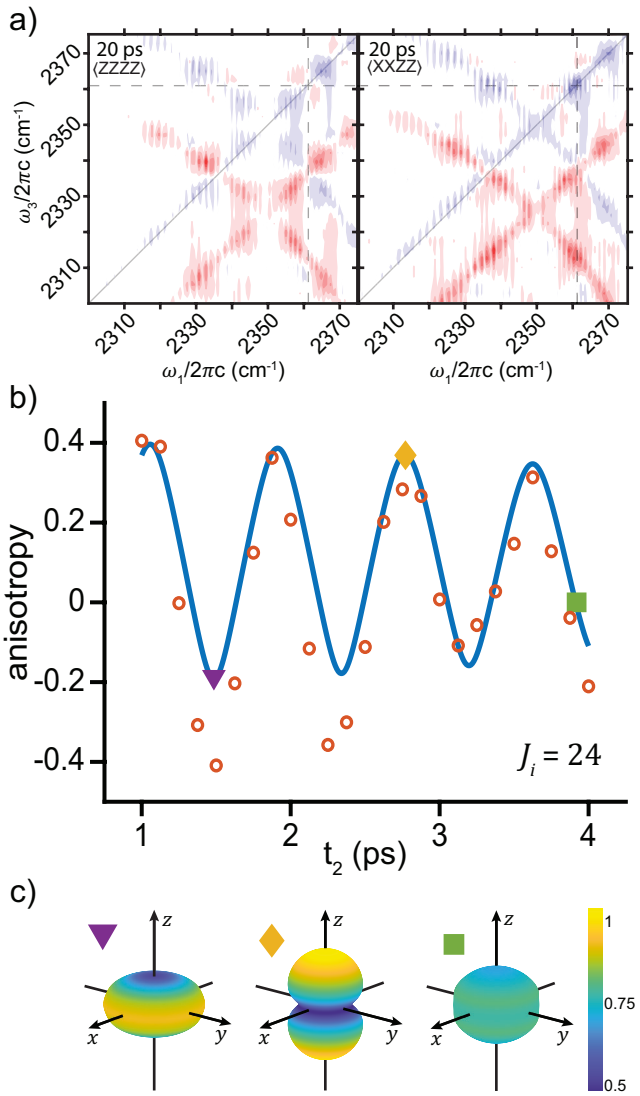

Figure 3: (a) When a peak is at a maximum in the perpendicular spectrum the same peak in the parallel spectrum is at a minimum, which causes the experimental anisotropy (orange circles, b) of the $J = 24$ peak in the RR-quadrant to oscillate between a maximum of 0.4 and a minimum of -0.4. The theoretical anisotropy (blue line) oscillates between 0.4 and -0.2. The probability density of the rotational wavefunction (Eq. 6) extends along the Z-axis when the anisotropy is at a maximum (yellow triangle), is stretched into the XY-plane when the anisotropy is negative (purple triangle), and is spherical when the anisotropy is zero (green square).

very close to the ideal value, 0.4, at all points of the spectrum. As the time delay increases, the anisotropy oscillates (Figure 3b), and the frequency of oscillation increases as a function of the initial value of J. For example, when $J = 24$, the anisotropy in the RR-quadrant oscillates with a $\sim$900 fs period (Figure 3b).

This beating pattern in the rotational anisotropy was not reported in N_2O, presumably because the rotational lines were not resolved. Due to the inversion symmetry of CO_2(g), only half of the rotational levels can be occupied, which increases the spacing in the rotational-vibrational spectrum from $2\tilde{B}(N_2O) = 2(0.419\,\mathrm{cm}^{-1}) = 0.838\,\mathrm{cm}^{-1}$ to $4\tilde{B}(CO_2) = 4(0.391\,\mathrm{cm}^{-1}) = 1.564\,\mathrm{cm}^{-1}$. This spacing is large enough to be resolved in our instrument in the ω_1-axis. We observe additional dynamics that were not visible in the N_2O spectra because overlapping rotational peaks cause interference from different pathways.

The pronounced beating patterns come from rotational coherences during the population time, t_2. From the set of 36 double-sided Feynman diagrams, there are multiple pathways that can contribute to each peak along the diagonal and anti-diagonal. Some of these pathways place the system in a time-dependent rotational coherence, not a time-independent population (Figure 1f). In 4 of 6 diagrams that contribute to peaks in the RR-quadrant (R_1, R_2, R_4, and R_5), the system is in a population during t_2, for example $|0, J\rangle\langle 0, J|$. In the other 2 diagrams (R_4^{coh} and R_5^{coh}), however, the system is in an interstate coherence during t_2, $|0, J+2\rangle\langle 0, J|$ or $|1, J+1\rangle\langle 1, J-1|$. We use the term interstate coherence (Ref.[6] p. 79) to distinguish the purely rotational coherences that evolve during t_2 from the rotational-vibrational coherences that oscillate during t_1 and t_3. These coherences oscillate with the difference of the frequencies of the rotational transitions, $\omega_{J,J+2}$ and $\omega_{J+1,J-1}$. The intensities of the peak in the $\langle ZZZZ\rangle$ spectrum and $\langle XXZZ\rangle$ spectrum originating in a given initial angular momentum state oscillate at the same frequency but shifted in phase, varying as $\cos^2(\omega_{J,J'}t_2)$ and $\sin^2(\omega_{J,J'}t_2)$, respectively.

The angular momentum of the light field can either increase or decrease the angular momentum of the CO_2, which ultimately dictates which diagrams cause interstate coherences.

Because linearly polarized light contains both left- and right-handed circularly polarized components, an electric field interaction in the Feynman diagram can either increase or decrease J depending on the initial value of m, m_i. For example, in R_5 (Figure 1f), the interactions all correspond to interacting with the same handedness of light – all right circularly polarized light if $m_i > 0$ or all left if $m_i < 0$. The first and third arrows going in on the left side of the diagram cause $\Delta J = +1$, and the second and fourth arrows going out cause $\Delta J = -1$. In this way, for each Feynman diagram, the ΔJ is determined by m_i, the direction of the arrow (the field or its conjugate), and if the arrow is on the right or left of the diagram. As another example, in R_5^{coh} (Figure 1f), the diagrams mix interactions with left and right circularly polarized light. The first arrow (in) and second arrow (out) on the left cause $\Delta J = +1$, so they have opposite handedness. Similarly, the third (in) and fourth (out) arrows both cause $\Delta J = -1$. In general, all diagrams that cause interstate coherences involve interactions with a mixture of right- and left-handed circularly polarized electric fields.

Nonlinear response function theory quantitatively reproduces the structure of the 2D-IR spectra (Figure 2, bottom). Working in the basis of rotational-vibrational levels and parameterizing the Hamiltonian against the linear and 2D-IR spectra, we solved for the spectrum by adding the contribution of each thermally populated rotational level (up to $J = 50$ and $m = -J, \ldots, J$) using well-documented approaches.[6] The major differences are that, rather than the usual 6 Feynman diagrams for each oscillator, there are 36, that the appropriate direction-dependent transition dipole moments[10–12] are used, and that the spectrum sums over the $(J + 1)^2 \approx 2600$ thermally occupied states ($\sim$93 600 Feynman diagrams total).

The simulations capture not only the overall shape of the spectra but also many subtle features (Figure 2, bottom). These features include the X-shapes, the curvature of the bands in the anti-diagonal direction, the beating structures, and the phase-twisted lineshapes (which are evident in the spectra as positive features (red) surrounding the negative peaks (blue).

The simulations also clarify that the origin of the beats are due to the rotational wavepackets launched by the pump pulses. The first pump pulse coherently excites many rotational transitions, which freely evolve during the coherence time, t_1. The Fourier transformation of t_1 spreads these frequency components out along the ω_1-axis. The second electric field interaction transfers the coherences to populations as well as interstate coherences. Immediately after the second pump pulse interacts with the system ($t_2 \approx 0$), the rotational wavepackets are completely in phase with one another, the peak intensities match the Boltzmann distribution, and there are no evident oscillations (Figure 2, bottom). At 8 ps, 20 ps and 40 ps, the wavepackets have different phases because each interstate coherence oscillates at a slightly different frequency (in fact, two closely spaced frequencies).

Due to the quantized rotational spectrum, rotational wavepackets can periodically rephase in a rotational revival. The CO_2 rotational wavepackets experience a full revival at a revival time of $T_r = h/2B(CO_2) \approx 42.7\,\text{ps}$,[13–19] as well as partial revivals at $nT_r/4$, where $n = 1, 2, 3, \cdots$. The prominent beat pattern in the 2D spectrum at 8 ps disappears near a quarter of the rotational revival time ($\sim$10 ps) because the rotational wavepacket has partially rephased (Figure 2). These two time points demonstrate rovibrational 2D-IR spectroscopy's ability to capture rotational wavepacket behavior at different stages of dephasing and rephasing. Where frequency integrated experiments like impulsive Raman scattering[13,20,21] detect the effect of the rotational alignment of all pumped molecules on the probe beam, 2D-IR spectroscopy separates the individual components of the wavepacket, providing insight into molecules in specific initial angular momentum states.

The rotational wavepacket shows the rotational alignment (Figure 3c) and explains the oscillations in the rotational anisotropy. The square of the rotational wavefunction displayed is the coherent superposition of all transition dipole weighted excitations from a particular

initial angular momentum state, $|J_i, m\rangle$. The relevant rotational wavefunctions are

$$\psi_1(t, J_i, m) = \psi_4(t, J_i, m) = Y^m_{J_i+1} e^{-iE_{J_i+1}t/\hbar}, \tag{2}$$

$$\psi_2(t, J_i, m) = \psi_5(t, J_i, m) = Y^m_{J_i} e^{-iE_{J_i}t/\hbar}, \tag{3}$$

$$\psi_4^{\mathrm{coh}}(t, J_i, m) = \frac{1}{\sqrt{2}} \left(Y^m_{J_i+1} e^{-iE_{J_i+1}t/\hbar} + Y^m_{J_i-1} e^{-iE_{J_i-1}t/\hbar} \right), \tag{4}$$

$$\psi_5^{\mathrm{coh}}(t, J_i, m) = \frac{1}{\sqrt{2}} \left(Y^m_{J_i+2} e^{-iE_{J_i+2}t/\hbar} + Y^m_{J_i} e^{-iE_{J_i}t/\hbar} \right), \tag{5}$$

where Y^m_J is the spherical harmonic corresponding to the eigenstate $|J, m\rangle$ and E_J is its energy. The probability density is then

$$\begin{aligned} |\Psi(t, J_i)|^2 = \sum_{m=-J_i}^{J_i} \Big[& |\psi_1(t, J_i, m)|^2 + |\psi_2(t, J_i, m)|^2 \\ & + |\psi_4(t, J_i, m)|^2 + |\psi_5(t, J_i, m)|^2 + |\psi_5^{\mathrm{coh}}(t, J_i, m)|^2 \Big] \\ & + \sum_{m=-(J_i-1)}^{J_i-1} |\psi_4^{\mathrm{coh}}(t, J_i, m)|^2. \end{aligned} \tag{6}$$

When the probability density of the rotational wavefunction is peaked along the Z-axis (yellow diamond), the anisotropy is near its maximum value of 0.4. As the rotational coherence evolves, the nuclear wavefunction flattens in the XY-plane (purple triangle) and the anisotropy reaches its most negative value. The experimental value approaches -0.4 where the calculation is bounded by -0.2. We note that the precise value of the anisotropy extracted from the experiment when the anisotropy is negative (S_{ZZZZ} is small) is sensitive to baseline artifacts due to the long wings of other transitions as well as the exact detuning of the rotational line and the frequency sampled by the experiment. When the rotational wavefunction is roughly spherical, the rotational anisotropy is close to 0 (green square).

The rotational structure imprinted in the 2D-IR spectra can be completely eliminated when the pump and probe pulses are at the "magic angle," $M = 54.7°$ (Figure 4), denoted $\langle MMZZ \rangle$. In this polarization condition, each direction in the lab-frame, X, Y, and Z,

contributes equal intensity to the spectra, and the spectra are proportional to the isotropic tensor component of the system response.[22] The beating patterns are suppressed, and the longer timescale changes in the 2D-IR lineshape become more clearly visible.

The 2D-IR spectra change shape as each peak broadens in ω_3 as a function of time (Figure 4). Each slice along ω_1 is proportional to the joint probability density of a molecule to have a certain final J_f at time t_2, given that it had a certain initial J_i at time 0 (Figure 4). Slices of the spectrum show J_f ranging from 0 to 34. The change in linewidth is due to inelastic scattering of the CO_2 molecules that cause a change in J. CO_2 has a mean free flight time of 84 ps at 1 atm and room temperature, and a quarter of all molecules experience a collision within 25 ps, while three-quarters collide within 110 ps.[23,24] As collisions during t_2 randomize the angular momentum, transitions to many other angular momenta become possible, and the sharp X-shaped bands in the 2D-IR spectrum become broad distributions. Due to our limited resolution in ω_3, the bands look like vertical stripes.

At early waiting times, each slice shows a peaked distribution centered at $\omega_3 \approx \omega_1$ (Figure 4, bottom). The initial population relaxes to a broad, Boltzmann distribution on the timescale of $t_2 \approx 100$ ps (Figure 4b).

Slices at ω_1 frequencies corresponding to $J = 8$ (Figure 4b), $J = 18$ (Figure 4c), and $J = 26$ (Figure 4d) were fit to the sum of a Lorentzian and a Boltzmann distribution. The center frequency for the Lorentzian was fit at the earliest t_2 and then fixed for longer t_2 times. The amplitude and width of the Lorentzian distribution and amplitude of the Boltzmann distribution were varied to find the best fit as a function of t_2. The narrowest features that can be resolved at early t_2 are limited by the resolution of the spectrograph and camera ($2.8\,cm^{-1}$). For each slice, the Lorentzian broadens while its amplitude decreases with t_2 due to collisions with small transfers of angular momentum. The Lorentzian component does not shift substantially as a function of time, which is inconsistent with many collisions causing a gradual, complete loss of angular momentum. Instead, the amplitude of the Boltzmann distribution increases with t_2 from approximately zero at $t_2 = 200$ fs to dominating the spec-

trum by 250 ps due to collisions with large transfers of angular momentum. The spectra thus demonstrate the potential to directly measure J-dependent angular momentum scattering.

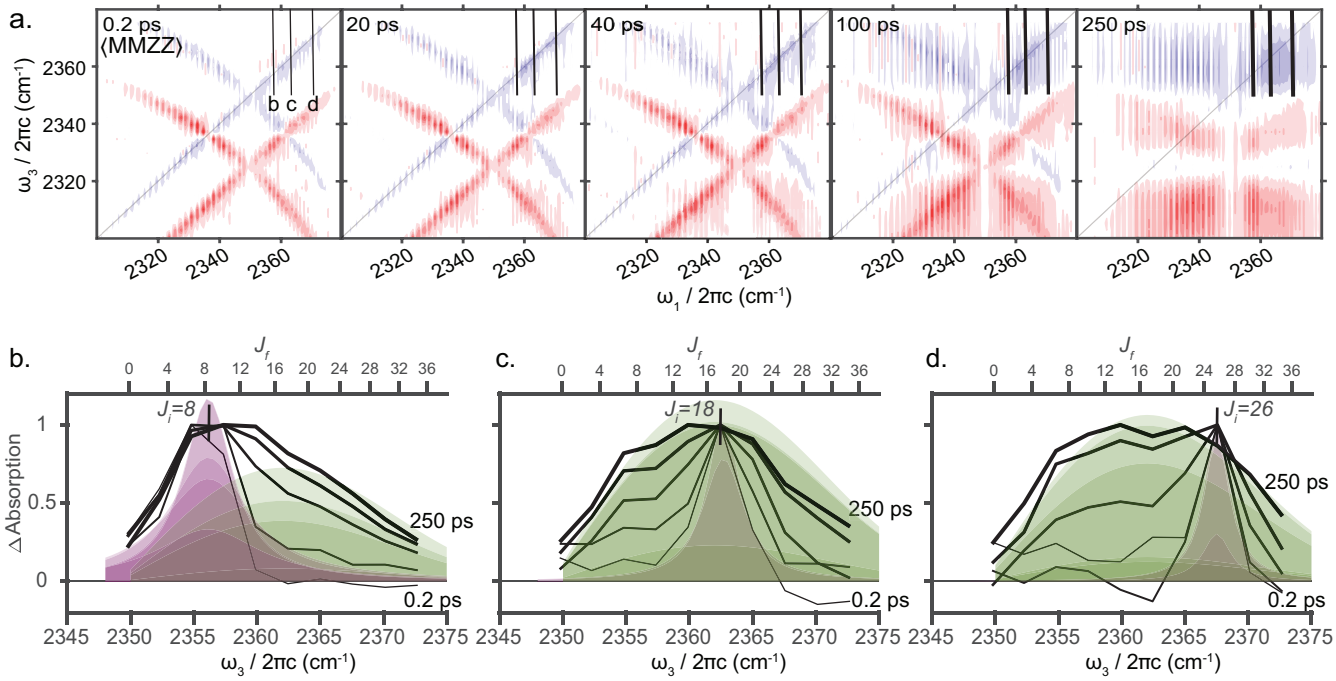

Figure 4: The magic angle polarization conditions suppress orientational beating and reveal J-scrambling in the 2D-IR spectra. (a) This is indicated by broadening of the rotational peaks along the ω_3-axis with increasing t_2. (b-d) A linear combination of a Lorentzian and a Boltzmann distributions qualitatively fit slices taken at the frequency corresponding to (b) $J_i = 8$, (c) $J_i = 18$, and (d) $J_i = 26$ along the ω_1-axis at $t_2 = 0.2$ ps, 20 ps, 40 ps, 100 ps and 250 ps. The Lorentzian contribution (purple) decreases and the Boltzmann contribution (green) increases from $t_2 = 0.2$ ps to 250 ps. The value of the corresponding initial rotational quantum number is shown in the top X-axis.

The 2D rotational-vibrational spectroscopy we have demonstrated is sensitive to changes in J but not to changes in m. The 2D-IR spectra change shape when the rotor scatters inelastically to a different J-level during t_2 because this collision changes the set of transitions that are possible during t_3. Elastic collisions have a smaller effect on the spectra. Though they change m, elastic collisions leave J and the transition energies during the final coherence time unchanged. Changes in m do change the transition intensities. The transition dipole depends on m, and we estimate that m-scrambling could decrease peak intensities by 15 – 20% of their initial intensities in the parallel spectrum. Separating this process from

vibrational relaxation, beating from the rotational wavepackets, and peak broadening due to inelastic collisions, however, is difficult.

New spectroscopic tools are needed to better reveal and control rotational wavepacket dynamics and angular momentum scrambling. Sophisticated laser fields may be able to coherently control the orientational distribution of free rotors.[14–18,25–34] Simultaneously, methods such as optical centrifuges[35] prepare rotors far from equilibrium, "super-rotors", with narrow distributions of angular momentum and orientational alignment. Transient IR absorption of individual rotational states then reveals the collisional dynamics of these "super-rotors".[36] Classical molecular dynamics simulations have proposed that highly rotationally excited molecules may undergo a metastable 'gyroscopic stage' in which they experience many collisions while maintaining the magnitude and orientation of their angular momentum,[37,38] which awaits experimental verification. Currently, 2D-IR spectroscopic techniques employing waveguides[39] and ring down cavities[8,9,40] are also being developed to measure the dynamics of trace gases. 2D-THz spectroscopy provides similar information in the time domain through purely rotational transitions.[41] Finally, multiple-comb spectroscopies are promising approaches to measure 2D spectra with high resolution in both ω_1 and ω_3.[8,9,40,42] In each of these areas, the essential physical processes we have presented here are likely to arise.

In conclusion, 2D-IR spectroscopy provides the power to observe and measure both angular momentum relaxation and rotational wavepacket dynamics for multiple rotational states of CO_2(g) simultaneously. This work does not change the interpretation of the classic rotational-vibrational spectrum, but it extends the spectrum into two dimensions, which reveals dynamics that are not detected in the linear absorption spectrum. We directly observe rotational wavepackets on the ground and first excited vibrational levels and inelastic angular momentum relaxation during t_2 for individual initial rotational states. Oscillations in the probability density due to interstate coherences during t_2 manifest as beating patterns in the 2D-IR spectra. Polarization-controlled 2D-IR experiments offer the power to quantify

the wavepacket dynamics or eliminate these features all together. 2D-IR spectroscopy has the ability to capture inelastic angular momentum scattering of molecules in varying angular momentum states simultaneously over several hundred picoseconds. For CO_2(g), the spectra at early times have narrow peaks that develop into a Boltzmann distribution as molecules in each initial angular momentum state thermalize. This behavior is likely generalizable to many different molecular systems.

As the field of ultrafast gas-phase spectroscopy advances, the phenomena reported in this work are likely to appear in these techniques. Changes in early time spectra are dominated by rotational coherences. As the waiting time increases and collisions begin to occur, angular momentum transfer drives spectral diffusion and becomes the dominant feature. Polarization-controlled experiments along with theoretical models describe these features and their physical origins.

Because of the intense, coherent excitation of many states simultaneously, the 2D-IR spectrum directly reveals the coherent and incoherent dynamics of molecules in many different J-levels simultaneously. 2D-IR spectroscopy could play a powerful role multiplexing the observation of the dynamics of molecules in the gas phase such as CO_2 at the interfaces or voids of carbon capture materials, molecules in highly excited rotational states such as optical centrifuges, and non-equilibrium states such as flames and explosions.

Experimental Methods

CO_2 (Matheson Tri-Gas, bone dry, 99.8% purity) was flowed ($1\,\mathrm{mL\,h^{-1}}$ to $10\,\mathrm{mL\,h^{-1}}$ to prevent loss of signal due to leakage) at a pressure of about 1 atm between two CaF_2 windows separated by a 12 µm Teflon spacer. The output passed through a deionized water-filled bubbler to visualize the flow of CO_2.

All FTIR samples were collected using a Nicolet 6700 (ThermoFisher Scientific) under nitrogen purge. A total of 64 scans each with a resolution of $0.25\,\mathrm{cm^{-1}}$ were collected. All

2D-IR spectra were collected using an ultrafast laser source (Coherent Vitesse/Coherent Legend Elite) with a center wavelength of 805 nm (120 fs pulse width, 5 kHz repetition rate). The home-built optical parametric amplifier (OPA)[43] employed parametric amplification in a type-II β-barium borate (BBO) crystal and, then, utilized difference frequency mixing in a type-I $AgGaS_2$ crystal to transform the light into the mid-infrared (λ = 3 µm to 6 µm). This method of generating femtosecond mid-infrared pulses was designed to suppress laser noise. For these experiments, the pulses were centered at ∼4.3 µm (200 cm^{-1} bandwidth, ∼1 µJ/pulse). Absorptive 2D spectra were collected in the pump-probe geometry, which allows for phase monitoring and scattering suppression.[44] The self-heterodyned signal field entered a spectrometer (Horiba, iHR320, grating 150 lines/mm) and was detected by a liquid nitrogen-cooled 2×32-channel mercury cadmium telluride (MCT) array detector (Infrared Systems Development). The final frequency axis, ω_3, was obtained directly from this array detector. The initial frequency, ω_1, was generated by scanning a Mach-Zehnder interferometer to control the time delay, t_1, between the two pump pulses (t_1 = −500 fs to 25 500 fs). Each interferogram was Fourier transformed to convert the signal from the time domain, t_1, into the frequency domain, ω_1. A wire grid polarizer and $\lambda/2$ waveplate were placed in the pump path. The wire grid polarizer was then set to 0° and 90° and the waveplate was set to optimize signal for parallel and perpendicular measurements, respectively. For magic angle measurements, the polarizer was set to 54.7°.

Acknowledgement

The authors acknowledge financial support from the National Science Foundation (CHE-1454105 and CHE-1954848). The authors also thank Mr. Thomas Gasmire of the University of Pittsburgh Dietrich School of Arts and Sciences Machine Shop, Dr. Thomas Brinzer, Dr. Clinton Johnson, Dr. Sunayana Mitra, Dr. C.J. Kelsheimer, and Mr. Tyler Parrack for their assistance.

References

(1) Mandal, A.; Ng Pack, G.; Shah, P. P.; Erramilli, S.; Ziegler, L. D. Ultrafast Two-Dimensional Infrared Spectroscopy of a Quasifree Rotor: J Scrambling and Perfectly Anticorrelated Cross Peaks. *Phys. Rev. Lett.* **2018**, *120*, 103401.

(2) Gordon, R. G. On the Rotational Diffusion of Molecules. *J. Chem. Phys.* **1966**, *44*, 1830–1836.

(3) McCaffery, A. J.; Alwahabi, Z. T.; Osborne, M. A.; Williams, C. J. Rotational Transfer, an Angular Momentum Model. *J. Chem. Phys.* **1993**, *98*, 4586–4602.

(4) AlWahabi, Z. T.; Besley, N. A.; McCaffery, A. J.; Osborne, M. A.; Rawi, Z. Dynamical Angular Momentum Models for Rotational Transfer in Polyatomic Molecules. *J. Chem. Phys.* **1995**, *102*, 7945–7952.

(5) Agrawal, P. M.; Agrawal, N. C.; Garg, V. Dynamical Constraints on the Angular Momentum Transfer in Rotationally Inelastic Molecular Collisions. *J. Chem. Phys.* **1985**, *83*, 4444–4447.

(6) Hamm, P.; Zanni, M. T. *Concepts and Methods of 2D Infrared Spectroscopy*; Cambridge University Press: New York, NY, 2011.

(7) Brinzer, T.; Berquist, E. J.; Ren, Z.; Dutta, S.; Johnson, C. A.; Krisher, C. S.; Lambrecht, D. S.; Garrett-Roe, S. Ultrafast Vibrational Spectroscopy (2D-IR) of CO2 in Ionic Liquids: Carbon Capture from Carbon Dioxide's Point of View. *J. Chem. Phys.* **2015**, *142*, 212425.

(8) Kowzan, G.; Allison, T. K. Controlling Rotationally-Resolved Two-Dimensional Infrared Spectra with Polarization. 2022; `https://arxiv.org/abs/2206.10492`.

(9) Kowzan, G.; Allison, T. K. Theory of Rotationally-Resolved Two-Dimensional Infrared Spectroscopy. 2022; `https://arxiv.org/abs/2206.10488`.

(10) Bernath, P. F. *Spectra of Atoms and Molecules*, 2nd ed.; Oxford University Press: United Kingdom, 2005.

(11) Fano, U.; Racah, G. *Irreducible Tensorial Sets*; Academic Press: New York, NY, 1959.

(12) Edmonds, A. *Angular Momentum in Quantum Mechanics*; Princeton University Press: Princeton, NJ, 1957.

(13) Bartels, R. A.; Weinacht, T. C.; Wagner, N.; Baertschy, M.; Greene, C. H.; Murnane, M. M.; Kapteyn, H. C. Phase Modulation of Ultrashort Light Pulses Using Molecular Rotational Wave Packets. *Phys. Rev. Lett.* **2002**, *88*, 4.

(14) Comstock, M.; Lozovoy, V. V.; Dantus, M. Rotational Wavepacket Revivals for Phase Modulation of Ultrafast Pulses. *Chem. Phys. Lett.* **2003**, *372*, 739–744.

(15) Hoque, M. Z.; Lapert, M.; Hertz, E.; Billard, F.; Sugny, D.; Lavorel, B.; Faucher, O. Observation of Laser-Induced Field-Free Permanent Planar Alignment of Molecules. *Phys. Rev. A - At. Mol. Opt. Phys.* **2011**, *84*, 1–6.

(16) Renard, V.; Renard, M.; Guérin, S.; Pashayan, Y. T.; Lavorel, B.; Faucher, O.; Jauslin, H. R. Postpulse Molecular Alignment Measured by a Weak Field Polarization Technique. *Phys. Rev. Lett.* **2003**, *90*, 4.

(17) Renard, V.; Renard, M.; Rouzée, A.; Guérin, S.; Jauslin, H. R.; Lavorel, B.; Faucher, O. Nonintrusive Monitoring and Quantitative Analysis of Strong Laser-Field-Induced Impulsive Alignment. *Phys. Rev. A - At. Mol. Opt. Phys.* **2004**, *70*, 1–9.

(18) Wu, C. Y.; Jiang, H. Y.; Wu, Z. F.; Gong, Q. H. Laser-Induced Alignment and Coulomb Explosion of CO2. *Chinese J. Chem. Phys.* **2009**, *22*, 571–576.

(19) Karras, G.; Hertz, E.; Billard, F.; Lavorel, B.; Hartmann, J.-M.; Faucher, O.; Gershnabel, E.; Prior, Y.; Averbukh, I. S. Orientation and Alignment Echoes. *Phys. Rev. Lett.* **2015**, *114*, 153601.

(20) Rosenberg, D.; Damari, R.; Kallush, S.; Fleischer, S. Rotational Echoes: Rephasing of Centrifugal Distortion in Laser-Induced Molecular Alignment. *J. Phys. Chem. Lett.* **2017**, *8*, 5128–5135.

(21) Rosenberg, D.; Damari, R.; Fleischer, S. Echo Spectroscopy in Multilevel Quantum-Mechanical Rotors. *Phys. Rev. Lett.* **2018**, *121*, 234101.

(22) Hochstrasser, R. M. Two-Dimensional IR-spectroscopy: Polarization Anisotropy Effects. *Chem. Phys.* **2001**, *266*, 273–284.

(23) Visco, P.; van Wijland, F.; Trizac, E. Collisional Statistics of the Hard-Sphere Gas. *Phys. Rev. E* **2008**, *77*, 041117.

(24) Paik, S. T. Is the Mean Free Path the Mean of a Distribution? *Am. J. Phys.* **2014**, *82*, 602–608.

(25) Granucci, G.; Persico, M.; Van Leuven, P. Alignment of Molecules in Pulsed Resonant Laser Fields. *J. Chem. Phys.* **2004**, *120*, 7438–7445.

(26) Lee, K. F.; Shapiro, E. A.; Villeneuve, D. M.; Corkum, P. B. Coherent Creation and Annihilation of Rotational Wave Packets in Incoherent Ensembles. *Phys. Rev. A - At. Mol. Opt. Phys.* **2006**, *73*, 1–6.

(27) Leibscher, M.; Averbukh, I. S.; Rabitz, H. Enhanced Molecular Alignment by Short Laser Pulses. *Phys. Rev. A - At. Mol. Opt. Phys.* **2004**, *69*, 10.

(28) Bisgaard, C. Z.; Viftrup, S. S.; Stapelfeldt, H. Alignment Enhancement of a Symmetric Top Molecule by Two Short Laser Pulses. *Phys. Rev. A - At. Mol. Opt. Phys.* **2006**, *73*, 1–9.

(29) Friedrich, B.; Herschbach, D. Alignment and Trapping of Molecules in Intense Laser Fields. *Phys. Rev. Lett.* **1995**, *74*, 4623–4626.

(30) Holmegaard, L.; Viftrup, S. S.; Kumarappan, V.; Bisgaard, C. Z.; Stapelfeldt, H.; Hamilton, E.; Seideman, T. Control of Rotational Wave-Packet Dynamics in Asymmetric Top Molecules. *Phys. Rev. A - At. Mol. Opt. Phys.* **2007**, *75*, 1–4.

(31) Sakai, H.; Safvan, C. P.; Larsen, J. J.; Hilligsøe, K. M.; Hald, K.; Stapelfeldt, H. Controlling the Alignment of Neutral Molecules by a Strong Laser Field. *J. Chem. Phys.* **1999**, *110*, 10235–10238.

(32) Dooley, P. W.; Litvinyuk, I. V.; Lee, K. F.; Rayner, D. M.; Spanner, M.; Villeneuve, D. M.; Corkum, P. B. Direct Imaging of Rotational Wave-Packet Dynamics of Diatomic Molecules. *Phys. Rev. A - At. Mol. Opt. Phys.* **2003**, *68*, 12.

(33) Normand, D.; Lompré, L. A.; Corneggia, C. Laser-Induced Molecular Alignment Probed by a Double-Pulse Experiment. *J. Phys. B At. Mol. Opt. Phys.* **1992**, *25*, L497–L503.

(34) Lee, K. F.; Villeneuve, D. M.; Corkum, P. B.; Shapiro, E. A. Phase Control of Rotational Wave Packets and Quantum Information. *Phys. Rev. Lett.* **2004**, *93*, 3–6.

(35) Karczmarek, J.; Wright, J.; Corkum, P.; Ivanov, M. Optical Centrifuge for Molecules. *Phys. Rev. Lett.* **1999**, *82*, 3420–3423.

(36) Murray, M. J.; Ogden, H. M.; Toro, C.; Liu, Q.; Burns, D. A.; Alexander, M. H.; Mullin, A. S. State-Specific Collision Dynamics of Molecular Super Rotors with Oriented Angular Momentum. *J. Phys. Chem. A* **2015**, *119*, 12471–12479.

(37) Khodorkovsky, Y.; Manson, J. R.; Averbukh, I. S. Modifying Molecule-Surface Scattering by Ultrashort Laser Pulses. *Phys. Rev. A* **2011**, *84*, 053420.

(38) Khodorkovsky, Y.; Steinitz, U.; Hartmann, J. M.; Averbukh, I. S. Collisional Dynamics in a Gas of Molecular Super-Rotors. *Nat. Commun.* **2015**, *6*, 7791.

(39) Greetham, G. M.; Clark, I. P.; Weidmann, D.; Ashfold, M. N. R.; Orr-Ewing, A. J.;

Towrie, M. Waveguide-Enhanced 2D-IR Spectroscopy in the Gas Phase. *Opt. Lett.* **2013**, *38*, 3596.

(40) Allison, T. K. Cavity-Enhanced Ultrafast Two-Dimensional Spectroscopy Using Higher Order Modes. *J. Phys. B At. Mol. Opt. Phys.* **2017**, *50*.

(41) Lu, J.; Zhang, Y.; Hwang, H. Y.; Ofori-Okai, B. K.; Fleischer, S.; Nelson, K. A. Nonlinear Two-Dimensional Terahertz Photon Echo and Rotational Spectroscopy in the Gas Phase. *Proc. Natl. Acad. Sci.* **2016**, *113*, 11800–11805.

(42) Lomsadze, B.; Cundiff, S. T. Multi-Heterodyne Two Dimensional Coherent Spectroscopy Using Frequency Combs. *Sci. Rep.* **2017**, *7*, 14018.

(43) Hamm, P.; Kaindl, R. A.; Stenger, J. Noise Suppression in Femtosecond Mid-Infrared Light Sources. *Opt. Lett.* **2000**, *25*, 1798–1800.

(44) Helbing, J.; Hamm, P. Compact Implementation of Fourier Transform Two-Dimensional IR Spectroscopy without Phase Ambiguity. *J. Opt. Soc. Am. B* **2011**, *28*, 171.